ACS NANO

www.acsnano.org

ARTICLE

Functional Asymmetry-Enabled Self-Adhesive Film via Phase Separation of Binary Polymer Mixtures for Soft Bio-Integrated Electronics

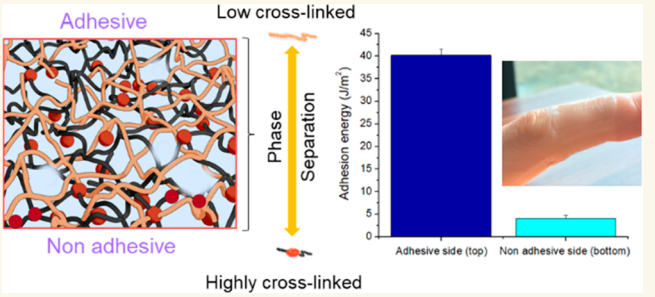
Moonjeong Bok,[§] Zhi-Jun Zhao,[§] Soon Hyoung Hwang, Junseong Ahn, Jiwoo Ko, Joo-Yun Jung, Jihye Lee, Sohee Jeon, and Jun-Ho Jeong*

Cite This: *ACS Nano* 2022, 16, 18157−18167

Read Online

ACCESS | Metrics & More | Article Recommendations | Supporting Information

ABSTRACT: **Biocompatible adhesive films are important for many applications (e.g., wearable devices, implantable devices, and attachable sensors). In particular, achieving self-adhesion on one side of a film with biocompatible materials is a compelling goal in adhesion science. Herein, we report a simple and easy manufacturing process using water-soluble hyaluronic acid (HA) that allows adhesiveness on only one side using binary polymer mixtures based on a phase-separation strategy with an elastomer. HA influx allows for the entangled polymer chains of the elastomer to spontaneously deform, permitting tunable mechanical elasticity, conformability, and adhesion. The proposed adhesive film enables the transfer of nanopatterning and the attachment of various surfaces without the use of additional chemicals. In addition, the film can be used for measuring epidermal biopotential and for skin fixation of drug devices. Therefore, the developed facile asymmetric adhesion can block the interferences of other materials on the unnecessary adhesion side, providing considerable potential for the development of functional, multifunctional, and smart bioadhesives.**



KEYWORDS: *asymmetric adhesion, hybrid elastomer, induced phase separation, e-skin, soft-biointegrated applications*

Smart bioadhesion has received considerable attention in the field of biointegrated electronics, including e-skin, e-tattoos, deformable sensors, and bioelectrodes.[1−6] For the development of such bioadhesives, extensive investigations have been made concerning materials and structures that can provide tunable mechanical properties and adhesion. The commonly reported processing method of synthetic bioadhesives ensures isotropic adhesion by applying various fabrication methods including cross-linking density control, side-group modification for covalent or noncovalent interactions, and introduction of dual-networking.[7−12] However, in the case of isotropic adhesion, the exposed adhesive component can easily collect impurities, thereby causing problems in practical applications, such as the instability of signal acquisition and poor anti-interference ability.[13−15] Therefore, the development of asymmetric films with adhesiveness on only one side should be considered. In addition, to meet the comfort and durability requirements of devices, specific asymmetric and mechanical properties are required. To fully realize this goal, functional adhesive films have been developed to mimic the surface structures of geckos, mussels, and octopuses from the structural point of view.[16−18] These approaches demonstrated impressive performance of reversible and repeatable skin adhesive patches for smart attachment devices, but they require a complex process and some features of their specific structures impose, to some extent, limitations on the contact surface.

From the material point of view, Fu et al. developed a superior asymmetrical adherent Janus hydrogel by applying a calcium chloride solution that conferred nonadhesiveness on top of the adhesive lignin hydrogel.[19] However, in this case, introduction of a specific functional group (solution) on the surface of the hydrogel is required to achieve asymmetric adhesion. In addition, Wan et al. developed an asymmetric elastomer by using two elastomer solutions that differed concerning the cross-linking density of the elastomer, that is, their adhesiveness/nonadhesiveness proprieties depending on the curing agent

Received: May 26, 2022
Accepted: October 10, 2022
Published: October 14, 2022



Downloaded via KOREA INST OF MACHINERY & MATERIALS on December 30, 2022 at 01:56:49 (UTC).
See https://pubs.acs.org/sharingguidelines for options on how to legitimately share published articles.

ACS Publications

© 2022 American Chemical Society

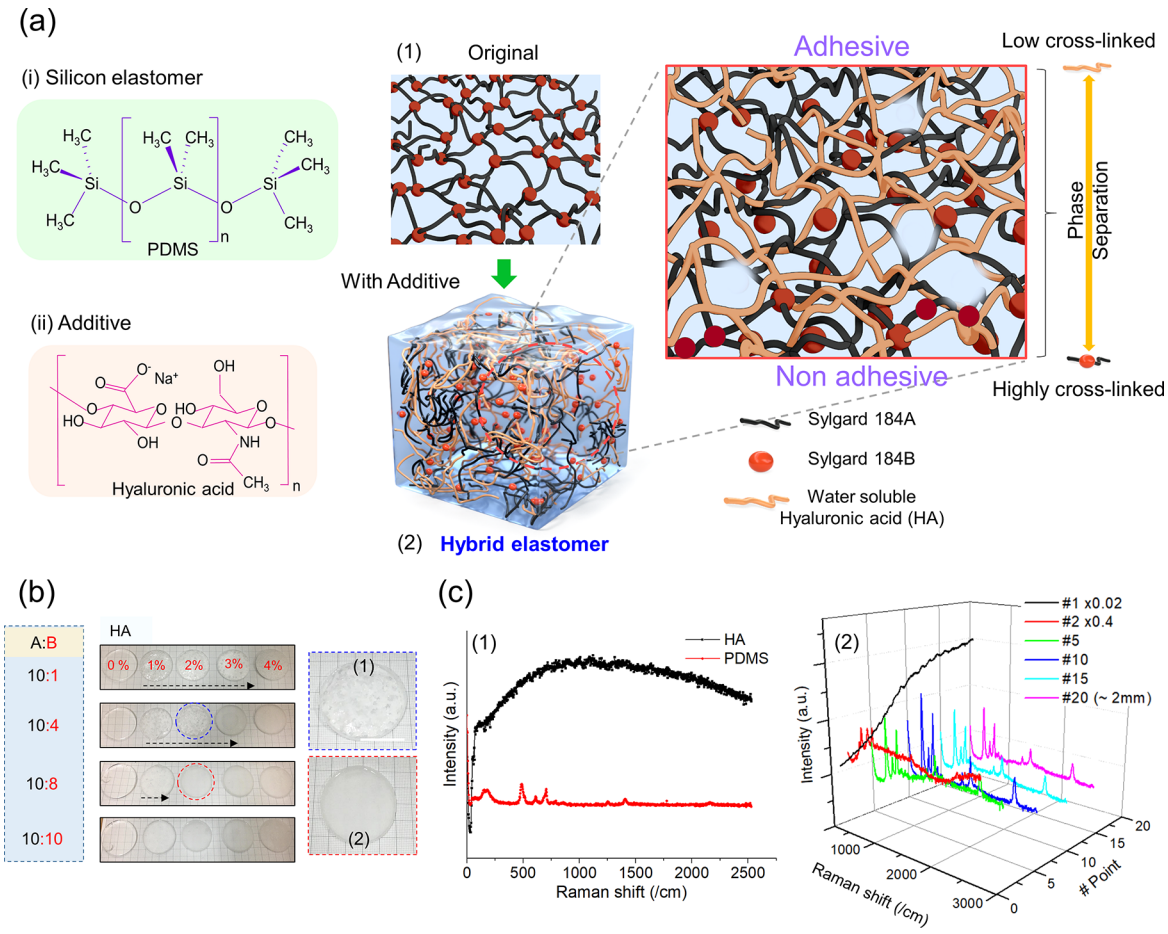


Figure 1. (a) Schematic diagram for manufacturing an HA−elastomer-based functional adhesive film. Chemical structure of (i) polydimethylsiloxane (PDMS) as a silicone elastomer and (ii) hyaluronic acid (HA) as an additive and expected structure of (1) the original silicone elastomer, well-packed state (hardened) and (2) the functional adhesive film with an additive (hybrid elastomer), in a loosely packed state (soft). The enlarged dotted lines describe the mechanism of the induced phase separation using additives for the formation of asymmetric adhesion. (b) Images of the fabricated films depending on the ratios of the curing agents and HA concentrations (scale bar = 2 cm), (1) porous and nonuniform film and (2) uniform film. (c) Measurements of the Raman spectrum to explain the mechanism of HA−elastomer-based functional adhesive films, (1) each HA and PDMS film and (2) cross-sectioned HA/PDMS composite film at different distances from the adhesive surface (×0.02, ×0.4: multiplied by the actual intensity, Figure S2).

ratio.[20] This method consists of two layers, and weakly bonded interface can impact on the stability and durability of the final product.

In general, the fabrication of single materials with asymmetric properties is complex, and difficult to precisely control. Thus far, developing an asymmetric functional adhesive film without requiring complex processing or using single solutions remains a great challenge.[21] Moreover, for large-scale industrialization/commercialization, inexpensive and small-scale production processing approaches are still warranted.

Cui et al. reported the formation of strong adhesion based on the application of a mixed solvent-induced phase separation strategy commonly used to produce nonadhesive hydrogels made of a polymer of acrylamide monomers.[22] This finding supports the possibility of using various soft/rigid hybrid devices in mixed solvents based on induced phase separation to achieve strong adhesive films. Hence, to achieve asymmetric adhesion with soft properties by dynamically changing the elasticity of the material, in this study, we propose the formation of asymmetric adhesion based on phase separation by physically mixing a hydrophilic HA polymer solution and a hydrophobic polydimethylsiloxane (PDMS) solution, which is expected to achieve the sensitive characteristics of adhesive/nonadhesive properties depending on the degree of cross-linking. HA is a natural nonirritating polysaccharide hydrophilic polymer that is used as an additive and is a highly stable material that can be applied in various fields, such as cosmetics, drug delivery, micro/nanopatterning-based wearables, and implantable devices.[23−26] Therefore, the present strategy is expected to produce a soft and flexible asymmetric adhesive film for easy application in wearable and attachable biomedical devices, with controllable surface properties related to adhesion, flexibility, transmittance, and thickness.

Herein, we describe a soft asymmetric adhesive film that was produced by inducing loosening of the entangled polymer chains of the elastomer through changes in the composition of the PDMS and aqueous solvents, as well as HA materials. In addition, the nanostructures were transferred onto the adhesive film surface without the use of auxiliary chemicals, demonstrating the broad applicability of the proposed adhesive film. The application of the HA−elastomer-based functional adhesive film for biointegrated devices demonstrates potential for two applications: (i) biosignal monitoring sensors to detect epidermal biopotential and (ii) topical skin use for fixing drug

https://doi.org/10.1021/acsnano.2c05159
ACS Nano 2022, 16, 18157−18167

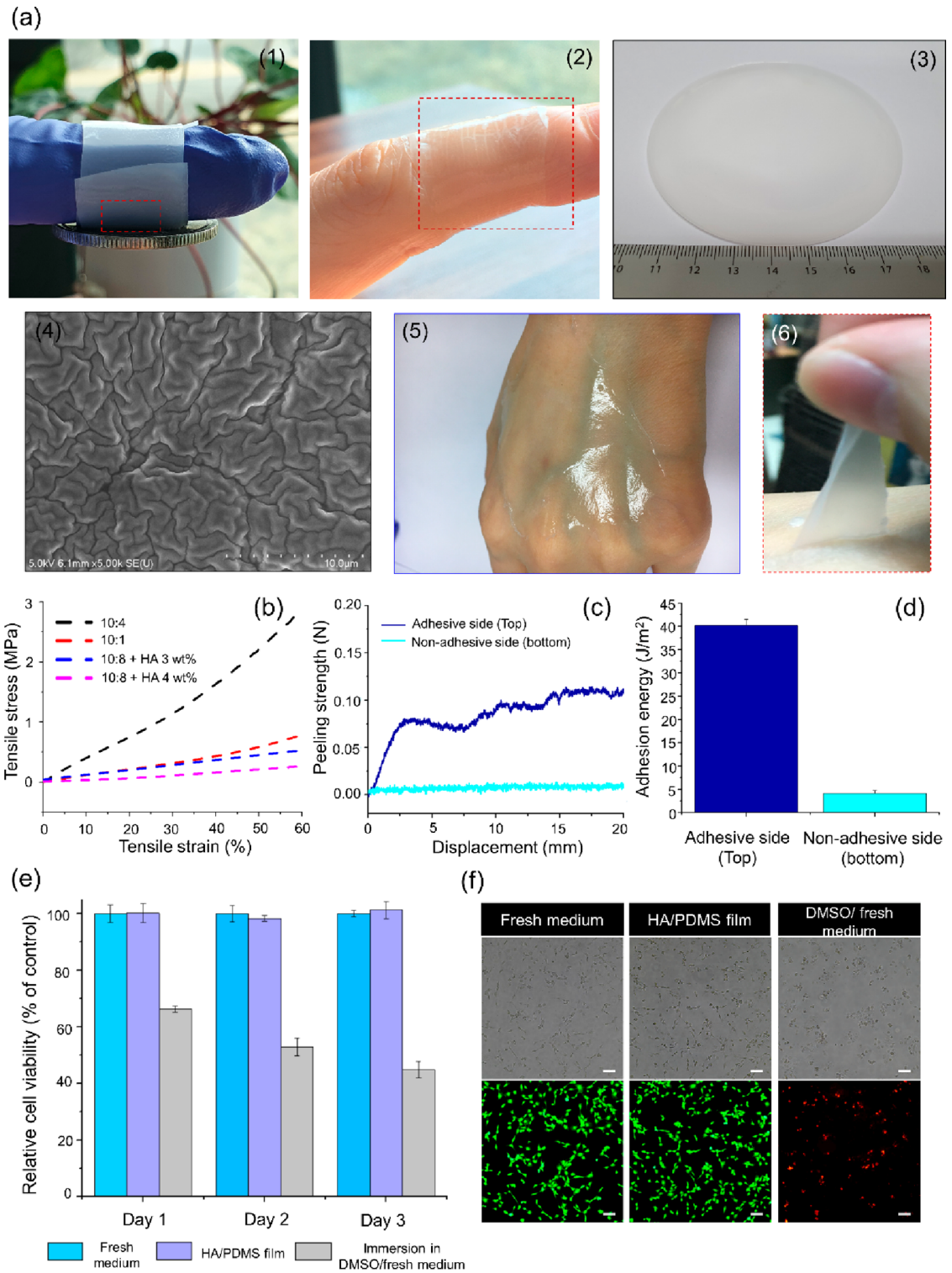


Figure 2. (a) Demonstration of the fabricated HA−elastomer-based functional adhesive film, (1) image of lifting a coin using the functional adhesive film, (2) very thin and transparent functional adhesive film, (3) a film with a diameter of approximately 7 cm, (4) scanning electron microscope image of the adhesive film, (5) micrometer-scale adhesive film attached to the back of a hand, and (6) image of pulling the film after attaching it to the skin to show adhesiveness. (b) Evaluation of stress−strain behavior of the HA−elastomer-based functional adhesive film. (c) Evaluation of the adhesive properties of the prepared film on the skin (peel strength-displacement curve from 90° peel tests). (d) Comparison of the adhesion energies of each side, calculated by F_{ave}/width from the peel strength−displacement curve (mean ± SD, n = 3). (e,f) Biocompatibility assessment of the developed film by (e) WST-1 assay using porcine dermal primary fibroblasts exposed to fresh medium, HA/PDMS film, or DMSO/fresh medium for 3 days and by (f) live/dead staining of porcine dermal primary fibroblast at day 1. Green and red colors represent live and dead cells, respectively (scale bar = 100 μm, mean ± SD, n = 3).

https://doi.org/10.1021/acsnano.2c05159
ACS Nano 2022, 16, 18157−18167

delivery devices. Therefore, we believe that the development of asymmetric adhesives based on phase separation presents a significant opportunity for the future development of next-generation smart adhesion materials and systems.

RESULTS AND DISCUSSION

Adhesion Mechanism of Elastomer Based on Hyaluronic Acid. Figure 1a presents a schematic diagram of the simple network structure of the easy fabrication process of the soft and flexible asymmetrically adhesive film consisting of two components: a hydrophobic polymer (PDMS) and a hydrophilic polymer (HA). PDMS, the most widely used silicone elastomer, is known to chemically cross-link to form an interconnected network with adjacent polymer chains that are sensitive to adhesive/nonadhesive properties depending on the cross-linking degree (Figure 1a,i). Therefore, PDMS can be combined with other constituent materials to impart elastomeric functions. These elastomers act as substrates or carriers, interconnecting the interface between the soft human body and high modulus components (for example, metal and electronic devices).[7,27,28] In turn, HA is a hydrophilic linear polysaccharide containing D-glucuronic acid, which combines N-acetyl-D-glucosamine as a disaccharide decomposing unit and has excellent biocompatibility and biodegradability,[23−26] making it a highly stable material (Figure 1a,ii). Figure 1a (1−2) presents the mechanism of generation of this composite film based on the incompatibility of the binary polymer mixtures. Generally, Sylgard 184 A and B components of the elastomer chemically cross-link, with increasing amounts of the cross-linking agent leading to a well packed and hardened product after curing; however, this final outcome will have impaired the ability to adhere to the substrate (skin; Figure 1a(1)). Hence, the degree of cross-linking can be controlled by changing the ratio of the silicone base to the curing agent, and the adhesion can be controlled through the degree of cross-linking, but this approach promotes symmetric properties. To overcome this limitation, we propose a mechanism using binary polymer mixtures based on phase-separation technique for fabrication of an asymmetric adhesive film by controlling cross-linking (Figure 1a (2)).

Surfactant-free phase separation is based on the fabrication of homogeneous single-phase solutions by mixing polymer and nonsolvent phases with different solubilities in solvents. With the evaporation of the solvent, the state is changed to two phases (the polymer-rich and polymer-low), and this fabrication is widely known as a method for designing porous polymers.[29−31] Here, we used HA polymers to disrupt the cross-linking of PDMS for asymmetric soft adhesion. This is possible because, in a physically mixed solution without surfactants, the affinity of the solution affects the network of the cross-linked polymers, causing them to separate and return to equilibrium. Moreover, these phase changes of the asymmetric film result from the gradient properties of phase separation in the mixed solution and are related to the casting conditions, including the compositional change of the casting solution, solution thickness, and temperature.[22,32] In other words, we created an asymmetric adhesive by inducing a gradual change in the degree of cross-linking in the elastomer solution through the inflow of added aqueous HA solution that interferes with the cross-linking of the two precursors of the chemically cross-linked elastomer (Sylgard 184 A and B). The adhesiveness appears only on one side (upper side), as shown by the enlarged dotted line in Figure 1a (2).

Optimization of the Casting Solution Composition. Figure 1b shows the appearance of the films produced using different compositions of the casting solution (concentration of HA solution, ratio of PDMS cross-linking agent). The same water volume was used for each HA solution, and the HA and PDMS solutions were mixed in a 1:1 ratio. Before adding the HA aqueous solution, the PDMS film was transparent regardless of the cross-linking agent, but the film became milky white after HA addition due to the distortion of the PDMS network structure. When the ratio of the cross-linking agent was low, as shown by the dotted line in Figure 1b (1), it was strongly entangled with the HA polymer to form a nonadhesive porous film. As the ratio of the cross-linking agent increased, it was increasingly uniformly mixed with the HA solution (Figure 1b (2)). Moreover, high water content relative to the HA amount resulted in the formation of a porous structure due to water loss during the curing process. For nonporous induced phase separation, low water content and a sufficient cross-linking agent are required. The point at which adhesion occurred was 184A/184B = 10:8, 3 wt % HA, and our manufactured film was fixed at 184A/184B = 10:8, 4 wt % HA. Therefore, the preparation of asymmetrically adhesive films using hydrophobic PDMS via induced phase separation strategy requires precise control of the compositional changes of the aqueous solvents and materials.

Figure 1c demonstrates the asymmetric mechanism of the HA/PDMS composite adhesive film. Raman spectroscopy was performed to confirm whether the added HA solution (as additive) could potentially alter the structural/chemical dynamics of the composite film. In addition, to characterize the distribution of the materials with the depth of the HA/PDMS composite adhesive film and asymmetric distribution, we measured the Raman spectra of cross-sections of the films. The Raman spectra of the pure HA and PDMS films were also measured for comparison. In the case of the pure HA film, there was no specific peak in the Raman spectrum, with specific peaks only appearing in the PDMS film, from 0 to 2526 cm^{-1} (Figure 1c (1)). As shown in Figure 1c (2) and Figure S2, HA addition significantly modified the shape of the Raman spectrum at each film depth. In the vicinity of the adhesive surface, the overall signal intensity was greater than that at other regions, and the PDMS peak dimmed. Conversely, moving away from the adhesive surface, the signal intensity decreased, and the PDMS peaks became clearer than in the vicinity of the adhesive surface. Therefore, the changes in the Raman signal with depth from the surface of the film support the rationale of the phase separation of the chemical cross-linking density distribution.

Adhesion Properties of Elastomer Based on Hyaluronic Acid. Figure 2 demonstrates the adhesive function of the patch produced. Figure 2a (1) demonstrates the ability to lift a coin using a thick adhesive film. In our case, it was possible to generate a transparent film (Figure 2a (2)), the size and thickness of which could be adjusted, as shown in Figure 2a (3,5). As the thickness decreased, it became optically transparent and allowed conformal attachment to the skin (Figure 2a (5)). A soft adhesive film was produced by the inflow of HA, and fine wrinkles were observed in the shape of the adhesive surface (Figure 2a (4)), which possibly resulted from interfacial instability caused by water evaporation from the mixed solution during the curing process.[33−35] Figure 2a (6) shows an image of a film that was pulled after attaching it to the skin to demonstrate the adhesion between the film and skin.

https://doi.org/10.1021/acsnano.2c05159
ACS Nano 2022, 16, 18157−18167

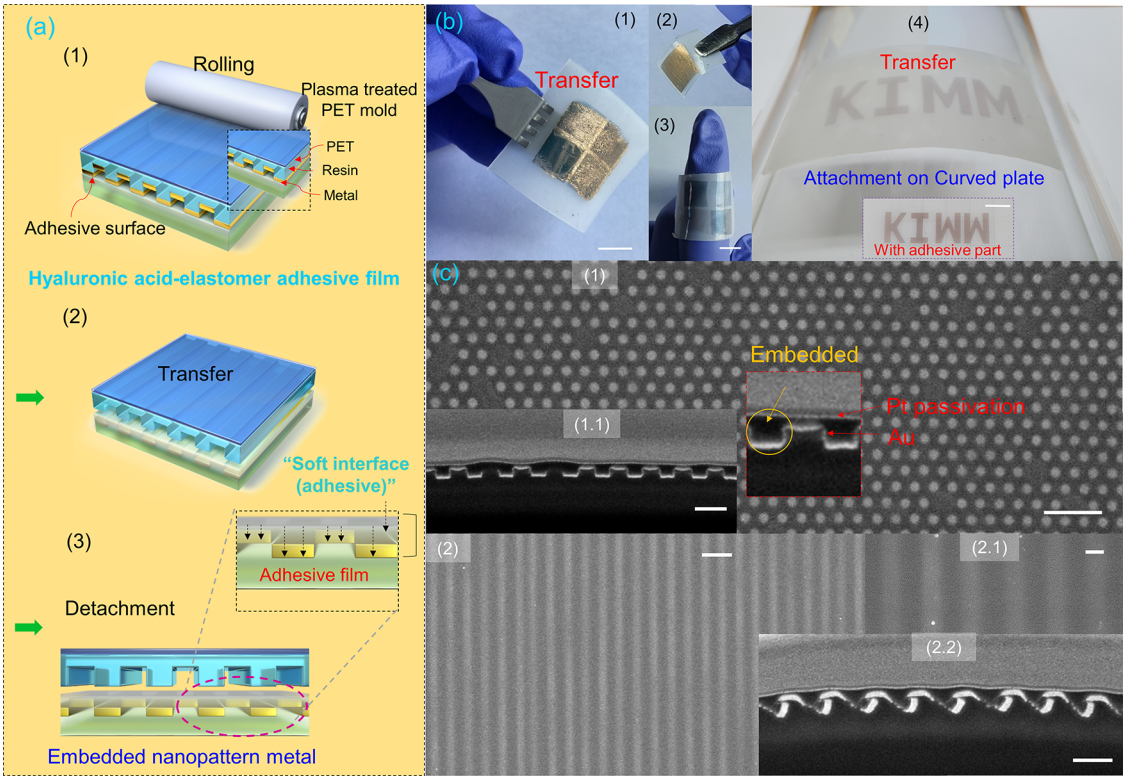


Figure 3. Adhesive-assisted transfer printing of nanopatterns using an HA−elastomer-based functional adhesive film. (a) Nano patterning transfer process on HA−elastomer-based functional adhesive film, (1) rolling after facing the adhesive surface and metal deposited on the nanostructure pattern film (in the case of the nanostructure film, the adhesion between the resin and metal was weakened by O_2 plasma treatment); (2) after rolling, the metal material moved into the adhesive film; (3) the metal was embedded in the adhesive surface. (b) Images after transfer on HA-elastomer-based functional adhesive film, (1−3) transferred patterns. (4) Pattern adherence to a curved surface after transferring the word "KIMM." The inset image shows the adhesive portion that transferred the pattern; scale bar = 1 cm. (c) Transferred surface morphology and focused ion beam cross-sectioned images, (1) dot pattern surface image, (1.1) cross-sectioned image of the dot pattern, with enlarged image showing the embedded metal (scale bars = (1) 1000 and (1.1) 300 nm); (2) line pattern surface image, (2.1) enlarged image showing the buried line pattern, and (2.2) cross-sectioned image of line pattern (scale bars = (2) 600, (2.1) 200, and (2.2) 400 nm).

In addition, we also compared the stress−strain behavior of the PDMS/HA composite film with that of PDMS-based elastomers with different mixing ratios between the cross-linking agent and silicone base. As shown in Figure 2b, when the curing agent ratio was increased from 10:1 to 10:4, the stress increased from approximately 0.7 to 2 MPa under the same 50% strain condition. Therefore, we confirmed that the stress applied under the same strain increases when the curing agent ratio is increased, and a larger stress can be applied to films resulting in a 10:8 ratio. When adding 3 and 4 wt % HA aqueous solution to the 10:8 curing agent ratio, the tensile stresses were greatly reduced to 0.3 and 0.2 MPa, respectively. Because the adhesive film must be a soft elastomer for application to wearable devices, we also specified the PDMS ratio (10:8) and the concentration of the HA (4 wt %) solution (Figures S4 and S5). Indeed, the hard elastomer was changed to a soft elastomer through the inflow of the HA aqueous solution, contrasting with the general method of softening the PDMS elastomer by changing the mixing ratio of the cross-linking agent/silicone base. Figure 2c,d shows the evaluation of the adhesive force of asymmetry characteristics through the peel test on the skin of the prepared film. The adhesion energy was defined as F_{ave}/w and calculated from the adhesion−displacement curve.[36] The adhesion energy of the upper surface was 40 J/m^2 and that of the lower surface was approximately 4 J/m^2; thus, demonstrating strongly asymmetric adhesion. Moreover, HA-based elastomers were created to be soft, with asymmetric adhesion, without changing the processing protocol in a major way.

In general, the adhesion mechanism between low-cross-linked PDMS and the skin (substrate) is mainly caused by van der Waals forces (physical adsorption).[7,37,38] Because the developed film also had adhesive properties due to the changes in the PDMS cross-linking by the inflow of HA aqueous solution, the adhesion between the skin and the film was derived from physical adsorption mediated by intermolecular interactions. Moreover, this soft film has a large contact area with the skin, thereby resulting in high intermolecular interactions per unit area and consequently enhancing its adhesiveness.[38]

The skin biocompatibility of the HA/PDMS film is important to avoiding side effects during use. To investigate the cytotoxicity of the HA/PDMS adhesive film, WST-1 cell proliferation and viability assays using porcine dermal primary fibroblasts were performed in fresh medium, HA/PDMS film, and in DMSO-added medium (Figure 2e,f). The *in vitro* biocompatibility of HA/PDMS film was comparable to that of the fresh medium condition, showing no noticeable decreased viability for 3 days. In contrast, DMSO-conditioned medium showed a stepwise toxicity in a time dependent manner, with *in vitro* viability reducing to less than 50% after 3 days. As shown in Figure 2f, bright field optical imaging and fluorescence live/dead staining confirmed the noncytotoxic effect of the HA/PDMS film as compared with the cytotoxicity of the DMSO-

https://doi.org/10.1021/acsnano.2c05159
ACS Nano 2022, 16, 18157−18167

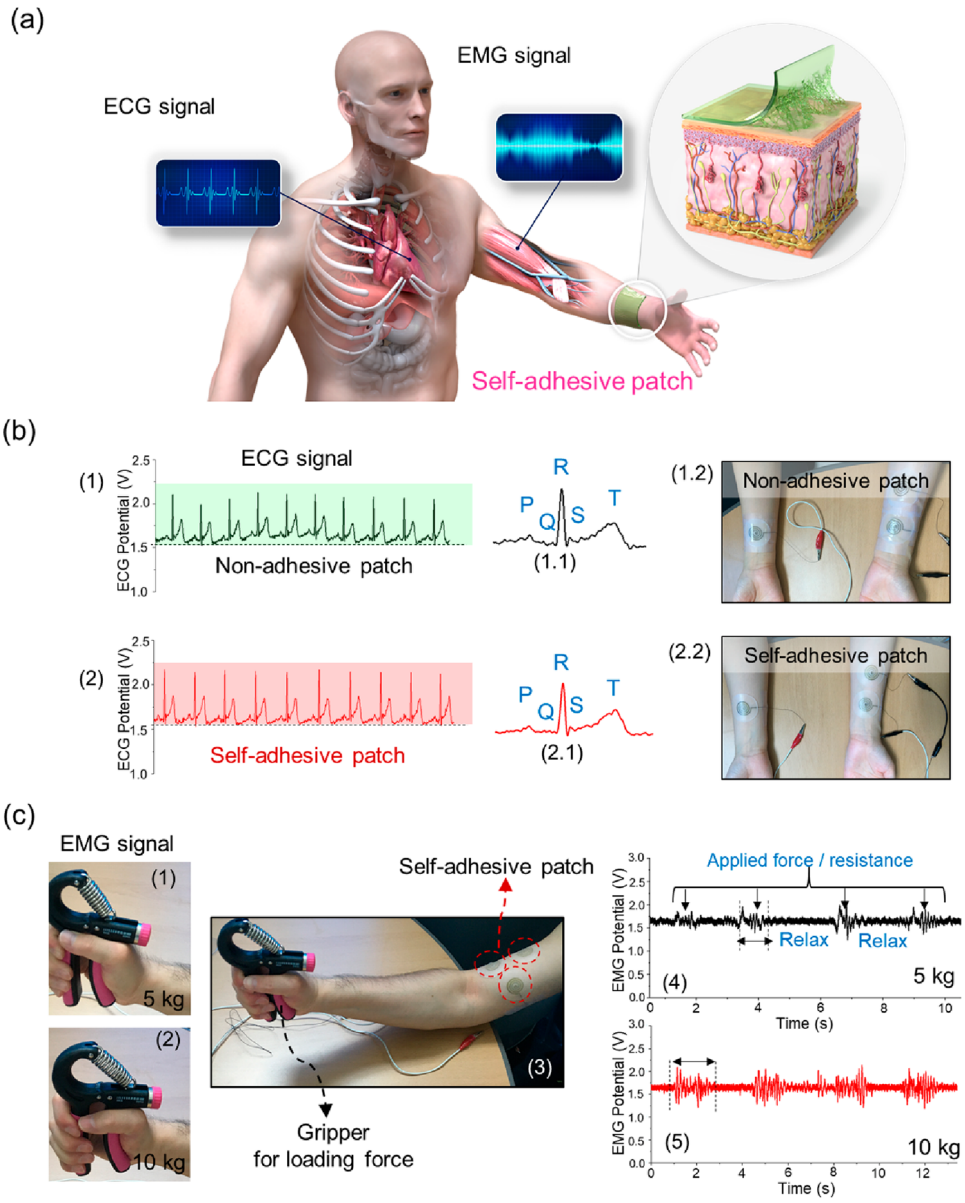


Figure 4. Adhesive-assisted biopotential measurement using an HA−elastomer-based functional adhesive film. (a) Schematic diagram for electrocardiography and electromyography (EMG) as an application for functional adhesive films. (b) Evaluation of electrocardiogram/heart rate. (1) Electrocardiogram (ECG) signal for nonadhesive film, (1.1) magnified ECG signal for nonadhesive film, (2) ECG signal for adhesive film, (2.1) magnified ECG signal for adhesive film, and (1.2, 2.2) experimental images for ECG. (c) Evaluation of EMG signal, (1) when 5 kg of force was applied to the gripper, (2) when 10 kg of force was applied to the gripper, (3) film attachment for EMG measurement, (4) EMG signal when 5 kg force was applied, and (5) EMG signal when 10 kg of force was applied.

conditioned medium. These results demonstrate the biocompatibility of the HA/PDMS film. Our biocompatible asymmetric adhesion, which is easy to fabricate, can block the attraction or interference of other materials due to unnecessary adhesion on the opposite side, which is essential for wearable device application, and could contribute to the secondary role of the device performance.

Adhesive-Assisted Transfer Printing of Nanopatterns. The fabrication of nanoscale patterns is becoming important for wearable-related electronic devices, such as small sensors, displays, energy harvesting devices that require high performance, and highly integrated devices.[24,39−42] Therefore, we propose the patterning of nanometal structures by controlling the adhesiveness of the developed wearable asymmetric adhesive film and the relative interfacial adhesion of the metal mold.

Figure 3 shows the application of nanopattern transfer using the adhesive properties of the fabricated film. Metal nanostructures were transferred onto the film using the nanoimprinting method and the adhesive components of the film. Herein, Au nanopatterns were fabricated using nanoimprinting and electron beam deposition and transferred to the developed film after weakening the adhesion between the resin and the deposited gold through O_2 plasma treatment (Figure 3a). The detailed process is provided in the Experimental Section. The surface of the adhesive film was soft; hence, the pattern could be embedded into the film (Figure 3a (3)). Figure 3b shows the transferred films. In particular, it can be seen in Figure 3b (4) that the letters "KIMM" transferred to the film surface and

https://doi.org/10.1021/acsnano.2c05159
ACS Nano 2022, 16, 18157−18167

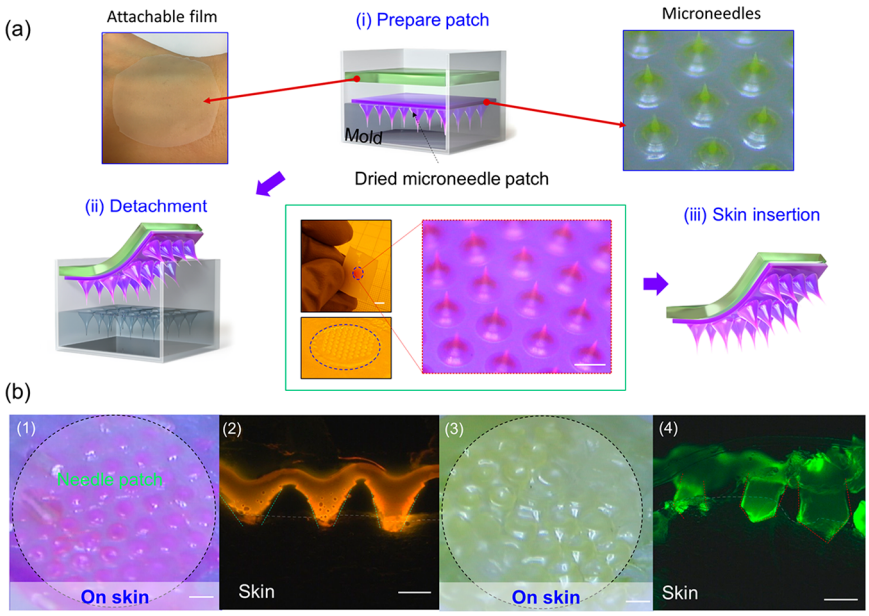


Figure 5. Adhesive-assisted drug delivery microneedle. (a) Microneedle transfer process onto an HA−elastomer-based functional adhesive film: (i) preparation of the cured microneedle in the mold and fabricated adhesive film, the arrows indicate an attachable film and microneedles; (ii) separation into the adhesive part of the fabricated film by contact with the microneedle; (iii) insertion of the microneedle with the application of the adhesive film onto the skin. The dotted line indicates an all-in-one attachable microneedles film (scale bars = 5 mm, 300 μm-enlarged image). (b) Actual images of transferred microneedles on the skin: (1, 3) optical image of the skin surface after needle transfer; (2, 4) fluorescent images of porcine cadaver skin after applying the adhesive-assisted drug delivery microneedle (red, 1,2-DNA/Rhodamine; green: 3,4-DNA/fluorescein isothiocyanate-dextran; scale bar = 200 μm).

attached to the curved surface. The inset image in Figure 3b (4) shows the pattern on the adhesive part, and Figure 3c shows the embedded patterns on the adhesive film. The embedded dot and line patterns on the surfaces were investigated using cross-section images. We confirmed that the patterns were well embedded in the film through the cross-section. Therefore, the adhesive layer transferred to the nanopattern onto the film and allowed the pattern to be embedded on the surface of the adhesive layer. The benefit based on the nanoprinting technology we demonstrated include, first, the adhesion for nanoprinting technology is based on the asymmetric adhesive film we have developed, which maintains biocompatible skin adhesion, and is harmless to the human body. Second, it is a wearable film; it is possible to embed the nanopattern into the film without chemical coating, high temperature, or pressure, and it may not affect the thickness of the film. Hence, this technology can have various applications for future nanodevices, such as security patterns for flexible and wearable devices, optics, and plasmonic technologies.

Adhesive-Assisted Biopotential Measurement. Adhesive films can be applied in wearable electrodes to measure epidermal biopotentials. Figure 4a shows the application of HA−elastomer-based functional adhesive films for electrocardiography and electromyography assessment. To record the electrocardiogram (ECG), the electrode film was placed as shown in Figure 4b (1.2,2.2), and the signals were compared based on the presence or absence of adhesion. In the case of nonadhesiveness, adhesion to the skin was not maintained, and tape was attached to the side for fixing the electrode (Figure 4b(1.2)). For the adhesive film, Figure 4b(2.2) shows the adhered electrode. The electrode film generated ECG signals with the expected waveform and a peak-to-peak voltage (QRS complex) of approximately 0.6 V. These ECG waveforms were similar to those obtained using a standard Ag/AgCl gel electrode. If the adhesion of the film was not uniform, the baseline ECG signal was irregular (Figure 4b (1)). In the case of an adhesive film (Figure 4b (2)), a clean ECG waveform and a stable baseline were observed.

Unambiguous identification of the ECG peak is important for diagnosing various health signal abnormalities in clinical settings; therefore, a wearable adhesive film is essential for measuring the epidermal biopotential. These adhesive films can also be used as electrode films for electromyography (EMG) to measure the action potentials generated by muscle fibers. As shown in Figure 4c, three adhesive films were attached to the muscle of one arm of the tester, and the EMG signal was observed by applying a force of 5 or 10 kg with a gripper. When force is applied using the gripper, the arm muscles contract to indicate a potential difference (EMG signal), which holds potential for applications in human−machine interfaces. In the present study, changes in muscle activity induced by contraction (as per the gripping force) were recorded using EMG signals. In addition, the film accurately detected the increase/decrease in the EMG signal during successive contraction/relaxation patterns. Muscle contraction is related to the force applied to the gripper, and the EMG signals indicated that increased muscle contraction was induced on applying a greater force to the gripper (Figure 4c (4,5)). However, for skin-contact electrodes in various environments, the high-conductivity wearable electrode manufacturing technology should be developed with low contact impedance and a higher signal-to-noise ratio, which was not investigated in this study. Moreover, to obtain a dry electrode more suitable for these epidermal electrode devices, systematic research on the electrode manufacturing technology with low cost, flexibility, optical transparency, and high conformability to the skin should be performed in the future.

https://doi.org/10.1021/acsnano.2c05159
ACS Nano 2022, 16, 18157−18167

Adhesive-Assisted Microneedle Patch. Dissolving microneedles are a patch-type drug delivery system that requires an adhesive film that adapts well to the skin and does not easily fall off to achieve ideal penetration and fixation.[43,44] The developed film has the advantage that it can be integrated into the dissolving microneedle manufacturing process as a biocompatible asymmetric adhesive film, which is an essential element of such drug delivery systems. Figure 5a shows the process for combining microneedles and the prepared attachable film, and how to attach it to the skin. Overall, the microneedles were pressed vertically with an adhesive film, with the microneedles (diameter of approximately 5 mm) being transferred to the adhesive film. The enlarged image of Figure 5a shows an optical image that confirms the presence of the needle array before skin attachment, confirming that the microneedles were correctly transferred onto the adhesive film. In addition, all-in-one self-adhesive microneedle films were attached to the skin to confirm their applicability. Skin samples exposed to the adhesive film were observed under an optical microscope (Figure 5b (1,3)). The microneedle was transferred to the skin surface owing to its fine surface moisture. Next, to observe the shape of the needle in the skin when the adhesive needle film was attached to it, we imaged cross-sections of the skin tissue (Figure 5b (2,4)). These images were observed within a short time after cryo-sectioning, and the needle penetrated the skin, through the outermost layer of the skin. Therefore, our proposed all-in-one self-adhesive microneedle could be applicable on the skin to inject drugs.

CONCLUSION

This study presents an asymmetric film strategy using simple and easy fabrication of HA−elastomer, a skin-friendly adhesive with various applications based on the phase separation of binary polymer mixtures. According to the developed methodology, the excessive inflow of water-soluble HA into the elastomer lowers its cross-linking density as the entangled polymer chains spontaneously unravel, thereby modulating the mechanical elasticity, conformability, and adhesion of the elastomer, as well as exhibiting functional asymmetry-enabled adhesion. Therefore, we report that HA−elastomer-based functional adhesive films provide an asymmetric adhesion strategy for the application of efficient and biointegrated flexible wearable devices.

EXPERIMENTAL SECTION

Fabrication of the HA−Elastomer-Based Functional Adhesive Film. PDMS (Sylgard 184; Dow Corning, Midland, MI, USA) solution was prepared using a mixer at a weight ratio of Sylgard 184 base/Sylgard 184 curing agent of 10:8. A 4 wt % solution of HA powder (HA-TLM 20−40, 200−400 kDa; Bloomage Biotechnology Corporation, Jinan, China) dissolved in deionized water was stirred at room temperature (23 °C) at 450 rpm for 10 h. The prepared PDMS and HA solutions were mixed in a weight ratio of 1:1 using a high speed mixer for approximately 2 min, and the mixed solution was gently poured into a 2-in. (or 4-in.) Petri dish. Some bubbles on the surface of the poured solution were popped using a needle, and the dishes were dried at 75 °C for approximately 6 h. To produce a film thickness of several tens of micrometers, the prepared solution was poured onto a Si wafer and spin-coated at 500 rpm for 30 s. In the case of the spin-coated sample for the production of tens of micrometer-scale films, curing was not performed well, so the curing temperature was set to about 90 °C for within 10 h (the curing time may vary depending on the film thickness).

Raman Characterization. Raman spectra were recorded using a micro-Raman spectrometer (NOST Co., Seongnam, Korea) with an excitation laser wavelength of 532 nm and spectral resolution of 1.8−2.2 cm^{-1}. In addition, the excitation laser power was 3 mW, and the objective lens was 50× (NA = 0.5). The approximate measurement range was 0−2526 cm^{-1}. In the case of the HA/PDMS composite film, the cross-section was cut and measured at intervals of approximately 100 μm from the surface of the adhesive layer (within approximately 1 mm) to a depth of approximately 2 mm.

Mechanical Characterization. Tensile measurements were performed using an Instron Model 5848 Micro Materials Testing System (Instron, Norwood, MA, USA). A 5 N load cell was used, and the crosshead speed was 50 mm/min. The load cell was calibrated prior to testing.

Adhesion Force Characterization. In the 90° peeling experiment, the top surface that does not come into contact with the fixed substrate was attached to a thin stiff backing (Kapton film), which prevented the elongation of the fabricated film in the peeling direction. The adhesion of the HA/PDMS composite adhesive film to each substrate (glass, polyethylene terephthalate [PET] film, and skin) was measured with a peeling strength−displacement based on a tensile tester (Instron Model E3000LT Micro Materials Testing System, Instron). The adhesive properties for different values of curing time, temperature, and stability were measured using skin as a substrate. The adhesive energy was calculated by F_{ave}/width (w = 2 mm).

Rheology Assay for Viscosity Measurement. The viscosity of the mixed solution was measured using a rotational rheometer (Haake MARS IQ, Thermo Fisher Scientific, Waltham, MA, USA). The viscosity was used in a shear rate value of 50 1/s.

Biocompatibility Test. *In vitro* cytotoxicity of the HA/PDMS film was examined using porcine dermal primary fibroblasts (APURES, Pyeongtaek, Korea). WST-1 and live/dead assays were performed for both quantitative and qualitative analysis. In summary, 1×10^4 fibroblasts were seeded in 96-well plates for at least 24 h before analysis. Afterward, half of the cell medium was discarded and replaced with fresh medium, followed by the addition of HA/PDMS extract or 5% (v/v) DMSO to the culture. For analysis of cell survival and proliferation, a WST-1 assay was performed as follows. The cells were first washed with Dulbecco's phosphate-buffered saline three times and incubated with WST-1 solution for 4 h in the incubator while being protected from light. Then, the culture plate was analyzed at 450 nm using a microplate reader (Tecan, Männedorf, Switzerland). For the live/dead assay, the cells were first washed with Dulbecco's phosphate-buffered saline three times and then treated with calcein-AM (2 μM, Thermo Fisher Scientific) and ethidium homodimer-1 (4 μM, Thermo Fisher Scientific) in Dulbecco's phosphate-buffered saline. The cells were then incubated for 45 min at room temperature and then observed under a fluorescent microscope (Nikon, Tokyo, Japan).

Nanotransfer Printing on HA/PDMS Adhesive Film. For nanotransfer printing, we prepared Si stamps with different nanoline and nanodot patterns. RM-311 (Minuta Technology Co., Ltd., Osan, Korea) polyurethane resin was applied to the Si stamp. After that, the transparent PET film was covered with a Si stamp and uniformly compressed using a roller, and the film was cured by irradiation with an ultraviolet light source for 3 min. The PET film was then separated from the Si stamp, and gold was deposited on the imprinted PET mold with nanopatterns. To facilitate the transfer to the HA−elastomer film, O_2 plasma (50 sccm, 100 W) treatment was performed for approximately 15 min to weaken the adhesion between the resin and metal on the PET mold. Using the adhesive part of the prepared HA−elastomer film as a donor substrate facing the PET mold treated with O_2 plasma, the HA−elastomer film was transferred using a roller and then separated.

Epidermal Biopotential Measurement. The fabricated adhesive electrode film composition for detecting epidermal biosignals had a crossed electrode arrangement, and approximately 200 nm of silver was deposited on the electrode. ECG signals were obtained by attaching two adhesive electrode films inside of one wire, with one adhesive electrode on the other wrist. A commercial ECG sensor module (PSL-iECG2, Physiolab Co., Busan, Korea) was used to detect the ECG signal, and a PSL-DAQ signal data acquisition module (Physiolab) was used for data acquisition. For the EMG signals, an adhesive electrode film was attached to the forearm. A commercial EMG sensor module (PSL-iEMG2; Physiolab) was used to detect the EMG signal, with a data

https://doi.org/10.1021/acsnano.2c05159
ACS Nano 2022, 16, 18157−18167

acquisition module. For a good signal, the notch filter was adjusted to 60 Hz.

Application of the Drug Delivery Device. *Preparation of Microneedle As Drug Delivery Device.* For the fabrication of the microneedle array with a diameter of approximately 5 mm, a master fabricated by 3D printing was used. The microneedle was designed with a height of approximately 600−800 μm each and a tip radius of approximately 20 μm.

For DNA-based microneedle production as a drug-injecting device, a 3 wt % DNA solution was prepared by dissolving DNA (polymerized deoxyribonucleotide, sodium salt, low molecular weight, medical grade, extracted from salmon milt; HTL Biotechnology, Javené, France) in 10 mL of deionized water.

To visualize the microneedle insertion into the skin, the fluorescent dye rhodamine b (0.0025 g, molecular weight: 479.01; Sigma-Aldrich, St. Louis, MO, USA) and fluorescein isothiocyanate-dextran (0.0025 g, average molecular weight: 70 000; Sigma-Aldrich) were mixed with each prepared DNA solution to obtain a uniform mixed solution. Then, 1.5 mL of the mixed solution was poured into prepared molds and placed in a vacuum desiccator for 5 min to remove air bubbles. Subsequently, the mold was removed and air-dried to harden the preparation.

Microneedle Transfer. The dried microneedle film in the mold was vertically faced to the adhesive part of the prepared adhesive film, and the microneedle film was transferred onto the adhesive film (the force to pull the microneedle film onto the adhesive film needed to be greater than the force of the microneedle film holding it in the mold).

Skin Tissue Analysis. The thickness of porcine cadaver skin used in this study was 1 mm (Micropig; Medi Kinetics, Pyeongtaek, Korea). All skin samples were stored at 4 °C until use. This study was approved by the institutional animal care and use committee. After adjusting the initial moisture content of the skin surface to 20%−30%, an adhesive-assisted microneedle patch was applied to the skin with a load of 2 kg. With the patch attached over the skin, the samples were frozen using a freezing block and then cut into 10 μm sections in the direction of the z axis. The generated sections were then visualized using 10× and 20× magnifications in a fluorescence microscope.

ASSOCIATED CONTENT

Supporting Information

The Supporting Information is available free of charge at https://pubs.acs.org/doi/10.1021/acsnano.2c05159.

Additional details, including each PDMS, HA, and PDMS/HA solution (film); additional asymmetric properties characterization details; the energy dispersive spectrometric analysis for component analysis of PDMS/HA composite film; comparison of the adhesive properties of composite film composed of the different PDMS ratios; comparison of the viscosity of different PDMS/HA mixed solutions; comparative test of isotropic and anisotropic adhesion; the images after electrode deposition on film with/without HA solution; adhesion evaluation on different substrates; adhesion evaluation on curing time, temperature, and stability; assembly of a crossed electrode for biopotential measurement using the PDMS/HA composite film; summary of various symmetric/asymmetric adhesive films (PDF)

Demonstration of asymmetric adhesive properties of the film (MP4)

Demonstration of durability of the film on the finger movement (MP4)

Demonstration of water resistance of the film (MP4)

AUTHOR INFORMATION

Corresponding Author

Jun-Ho Jeong − *Nano-Convergence Manufacturing Systems Research Division, Korea Institute of Machinery and Materials, Daejeon 34103, South Korea;* orcid.org/0000-0003-0671-0225; Phone: +82-42-868-7604; Email: jhjeong@kimm.re.kr; Fax: +82-42-868-7123

Authors

Moonjeong Bok − *Nano-Convergence Manufacturing Systems Research Division, Korea Institute of Machinery and Materials, Daejeon 34103, South Korea*

Zhi-Jun Zhao − *Institute of Smart City and Intelligent Transportation, Southwest Jiaotong University, Chengdu, Sichuan 610097, China*

Soon Hyoung Hwang − *Nano-Convergence Manufacturing Systems Research Division, Korea Institute of Machinery and Materials, Daejeon 34103, South Korea*

Junseong Ahn − *Nano-Convergence Manufacturing Systems Research Division, Korea Institute of Machinery and Materials, Daejeon 34103, South Korea;* orcid.org/0000-0002-4090-5440

Jiwoo Ko − *Nano-Convergence Manufacturing Systems Research Division, Korea Institute of Machinery and Materials, Daejeon 34103, South Korea*

Joo-Yun Jung − *Nano-Convergence Manufacturing Systems Research Division, Korea Institute of Machinery and Materials, Daejeon 34103, South Korea*

Jihye Lee − *Nano-Convergence Manufacturing Systems Research Division, Korea Institute of Machinery and Materials, Daejeon 34103, South Korea*

Sohee Jeon − *Nano-Convergence Manufacturing Systems Research Division, Korea Institute of Machinery and Materials, Daejeon 34103, South Korea*

Complete contact information is available at: https://pubs.acs.org/10.1021/acsnano.2c05159

Author Contributions

[§]M.B. and Z.-J.Z. performed all experiments, analyzed the data, and wrote the paper. S.H.H., J.A., J.K., J.-Y.J., J.L., and S.J. discussed the results. J.-H.J. led the overall direction of the project. These authors contributed equally.

Notes

The authors declare no competing financial interest.

ACKNOWLEDGMENTS

This work was supported by the Center for Advanced Meta-Materials (CAMM), funded by the Ministry of Science, ICT and Future Planning, Korea, through the Global Frontier Project (CAMM-No. 2014M3A6B3063707), Ministry of Culture, Sports and Tourism and Korea Creative Content Agency (Project Number: R2022020033), Korea Evaluation Institute of Industrial Technology (KEIT) grant funded by the Korea government (MOTIE) (Project Number: 20018235) and the Fundamental Research Funds for the Central Universities (2682022CX071).

ABBREVIATIONS

ECG, electrocardiogram; EMG, electromyography; HA, hyaluronic acid; PDMS, polydimethylsiloxane; PET, polyethylene terephthalate

https://doi.org/10.1021/acsnano.2c05159
ACS Nano 2022, 16, 18157−18167

REFERENCES

(1) Drotlef, D. M.; Amjadi, M.; Yunusa, M.; Sitti, M. Bioinspired Composite Microfibers for Skin Adhesion and Signal Amplification of Wearable Sensors. *Adv. Mater.* **2017**, *29*, 1701353.

(2) Wang, Q.; Ling, S.; Liang, X.; Wang, H.; Lu, H.; Zhang, Y. Self-Healable Multifunctional Electronic Tattoos Based on Silk and Graphene. *Adv. Funct. Mater.* **2019**, *29*, 1808695.

(3) Zhang, L.; Ji, H.; Huang, H.; Yi, N.; Shi, X.; Xie, S.; Li, Y.; Ye, Z.; Feng, P.; Lin, T.; Liu, X.; Leng, X.; Li, M.; Zhang, J.; Ma, X.; He, P.; Zhao, W.; Cheng, H. Wearable Circuits Sintered at Room Temperature Directly on the Skin Surface for Health Monitoring. *ACS Appl. Mater. Interfaces* **2020**, *12*, 45504−45515.

(4) Zhang, W.; Zhang, L.; Liao, Y.; Cheng, H. Conformal Manufacturing of Soft Deformable Sensors on the Curved Surface. *Int. J. Extrem. Manuf.* **2021**, *3*, 042001.

(5) Xu, Z.; Chen, L.; Lu, L.; Du, R.; Ma, W.; Cai, Y.; An, X.; Wu, H.; Luo, Q.; Xu, W.; Zhang, Q.; Jia, X. A Highly-Adhesive and Self-Healing Elastomer for Bio-Interfacial Electrode. *Adv. Funct. Mater.* **2021**, *31*, 2006432.

(6) Zhu, J.; Zhou, H.; Gerhard, E. M.; Zhang, S.; Parra Rodriguez, F. I.; Pan, T.; Yang, H.; Lin, Y.; Yang, J.; Cheng, H. Smart Bioadhesives for Wound Healing and Closure. *Bioact. Mater.* **2023**, *19*, 360−375.

(7) Jeong, S. H.; Zhang, S.; Hjort, K.; Hilborn, J.; Wu, Z. PDMS-Based Elastomer Tuned Soft, Stretchable, and Sticky for Epidermal Electronics. *Adv. Mater.* **2016**, *28*, 5830−5836.

(8) Li, S.; Chen, N.; Li, X.; Li, Y.; Xie, Z.; Ma, Z.; Zhao, J.; Hou, X.; Yuan, X. Bioinspired Double-Dynamic-Bond Crosslinked Bioadhesive Enables Post-Wound Closure Care. *Adv. Funct. Mater.* **2020**, *30*, 2000130.

(9) Zhang, L.; Kumar, K. S.; He, H.; Cai, C. J.; He, X.; Gao, H.; Yue, S.; Li, C.; Seet, R. C.-S.; Ren, H.; Ouyang, J. Fully Organic Compliant Dry Electrodes Self-Adhesive to Skin for Long-Term Motion-Robust Epidermal Biopotential Monitoring. *Nat. Commun.* **2020**, *11*, 4683.

(10) Huang, W.; Cheng, S.; Wang, X.; Zhang, Y.; Chen, L.; Zhang, L. Noncompressible Hemostasis and Bone Regeneration Induced by an Absorbable Bioadhesive Self-Healing Hydrogel. *Adv. Funct. Mater.* **2021**, *31*, 2009189.

(11) Rahman, M. A.; Bowland, C.; Ge, S.; Acharya, S. R.; Kim, S.; Cooper, V. R.; Chen, X. C.; Irle, S.; Sokolov, A. P.; Savara, A.; Saito, T. Design of Tough Adhesive from Commodity Thermoplastics Through Dynamic Crosslinking. *Sci. Adv.* **2021**, *7*, No. eabk2451.

(12) Bu, Y.; Pandit, A. Cohesion Mechanisms for Bioadhesives. *Bioact. Mater.* **2022**, *13*, 105−18.

(13) Yan, L.; Yang, X.; Zhang, Y.; Wu, Y.; Cheng, Z.; Darling, S. B.; Shao, L. Porous Janus Materials with Unique Asymmetries and Functionality. *Mater. Today (Kidlington)* **2021**, *51*, 626−647.

(14) Wang, Q.; Pan, X.; Guo, J.; Huang, L.; Chen, L.; Ma, X.; Cao, S.; Ni, Y. Lignin and Cellulose Derivatives-Induced Hydrogel with Asymmetrical Adhesion, Strength, and Electriferous Properties for Wearable Bioelectrodes and Self-Powered Sensors. *Chem. Eng. J.* **2021**, *414*, 128903.

(15) Wu, X.; Guo, W.; Wang, L.; Xu, Y.; Wang, Z.; Yang, Y.; Yu, L.; Huang, J.; Li, Y.; Zhang, H.; Wu, Y.; Li, G.; Huang, W. An Injectable Asymmetric-Adhesive Hydrogel as a GATA6^{+} Cavity Macrophage Trap to Prevent the Formation of Postoperative Adhesions after Minimally Invasive Surgery. *Adv. Funct. Mater.* **2022**, *32*, 2110066.

(16) Jin, K.; Cremaldi, J. C.; Erickson, J. S.; Tian, Y.; Israelachvili, J. N.; Pesika, N. S. Biomimetic Bidirectional Switchable Adhesive Inspired by the Gecko. *Adv. Funct. Mater.* **2014**, *24*, 574−579.

(17) Baik, S.; Kim, D. W.; Park, Y.; Lee, T. J.; Ho Bhang, S.; Pang, C. A Wet-Tolerant Adhesive Patch Inspired by Protuberances in Suction Cups of Octopi. *Nature* **2017**, *546*, 396−400.

(18) Ma, Y.; Ma, S.; Wu, Y.; Pei, X.; Gorb, S. N.; Wang, Z.; Liu, W.; Zhou, F. Remote Control Over Underwater Dynamic Attachment/Detachment and Locomotion. *Adv. Mater.* **2018**, *30*, 1801595.

(19) Fu, C.; Ni, Y.; Chen, L.; Huang, F.; Miao, Q.; Huang, L. Design of Asymmetric-Adhesion Lignin-Reinforced Hydrogels Based on Disulfide Bond Crosslinking for Strain Sensing Application. *Int. J. Biol. Macromol.* **2022**, *212*, 275−282.

(20) Wan, X.; Gu, Z.; Zhang, F.; Hao, D.; Liu, X.; Dai, B.; Song, Y.; Wang, S. Asymmetric Janus Adhesive Tape Prepared by Interfacial Hydrosilylation for Wet/Dry Amphibious Adhesion. *NPG Asia Mater.* **2019**, *11*, 1−9.

(21) Feng, L.; Shi, W.; Chen, Q.; Cheng, H.; Bao, J.; Jiang, C.; Zhao, W.; Zhao, C. Smart Asymmetric Hydrogel with Integrated Multi-Functions of NIR-Triggered Tunable Adhesion, Self-Deformation, and Bacterial Eradication. *Adv. Healthc. Mater.* **2021**, *10*, 2100784.

(22) Cui, W.; Zhu, R.; Zheng, Y.; Mu, Q.; Pi, M.; Chen, Q.; Ran, R. Transforming Non-Adhesive Hydrogels to Reversible Tough Adhesives *Via* Mixed-Solvent-Induced Phase Separation. *J. Mater. Chem. A* **2021**, *9*, 9706−9718.

(23) Kim, J.; Campbell, A. S.; de Ávila, B. E. F.; Wang, J. Wearable Biosensors for Healthcare Monitoring. *Nat. Biotechnol.* **2019**, *37*, 389−406.

(24) Ko, J.; Zhao, K. J.; Hwang, S. H.; Kang, H. J.; Ahn, J.; Jeon, S.; Bok, M.; Jeong, Y.; Kang, K.; Cho, I.; Jeong, J.-H.; Park, I. Nanotransfer Printing on Textile Substrate with Water-Soluble Polymer Nanotemplate. *ACS Nano* **2020**, *14*, 2191−2201.

(25) Bok, M.; Zhao, Z. J.; Jeon, S.; Jeong, J. H.; Lim, E. Ultrasonically and Iontophoretically Enhanced Drug-Delivery System Based on Dissolving Microneedle Patches. *Sci. Rep.* **2020**, *10*, 1−10.

(26) Ko, J.; Kang, H. J.; Ahn, J.; Zhao, Z. J.; Jeong, Y.; Hwang, S. H.; Bok, M.; Jeon, S.; Gu, J.; Ha, J.-H.; Rho, J.; Jeong, J.-H.; Park, I. Biocompatible Nanotransfer Printing Based on Water Bridge Formation in Hyaluronic Acid, and Its Application to Smart Contact Lenses. *ACS Appl. Mater. Interfaces* **2021**, *13*, 35069−35078.

(27) Zhang, K.; Kong, S.; Li, Y.; Lu, M.; Kong, D. Soft Elastomeric Composite Materials with Skin-Inspired Mechanical Properties for Stretchable Electronic Circuits. *Lab. Chip* **2019**, *19*, 2709−2717.

(28) Kim, D. C.; Shim, H. J.; Lee, W.; Koo, J. H.; Kim, D. H. Material-Based Approaches for the Fabrication of Stretchable Electronic. *Adv. Mater.* **2020**, *32*, 1902743.

(29) Danesh, E.; Ghaffarian, S. R.; Molla-Abbasi, P. Non-Solvent Induced Phase Separation as a Method for Making High-Performance Chemiresistors Based on Conductive Polymer Nanocomposites. *Sens. Actuators B Chem.* **2011**, *155*, 562−567.

(30) Khoryani, Z.; Seyfi, J.; Nekoei, M. Investigating the Effects of Polymer Molecular Weight and Non-Solvent Content on the Phase Separation, Surface Morphology and Hydrophobicity of Polyvinyl Chloride Films. *Appl. Surf. Sci.* **2018**, *428*, 933−940.

(31) Wan, C. T. C.; Jacquemond, R. R.; Chiang, Y. M.; Nijmeijer, K.; Brushett, F. R.; Forner-Cuenca, A. Non-Solvent Induced Phase Separation Enables Designer Redox Flow Battery Electrodes. *Adv. Mater.* **2021**, *33*, 2006716.

(32) Pervin, R.; Ghosh, P.; Basavaraj, M. G. Tailoring Pore Distribution in Polymer Films *Via* Evaporation Induced Phase Separation. *RSC Adv.* **2019**, *9*, 15593−15605.

(33) Zheng, S.; Huang, S.; Xiong, L.; Yang, W.; Liu, Z.; Xie, B.; Yang, M. Tunable Wrinkle Structure Formed on Surface of Polydimethylsiloxane Microspheres. *Eur. Polym. J.* **2018**, *104*, 99−105.

(34) Yang, S.; Khare, K.; Lin, P. C. Harnessing Surface Wrinkle Patterns in Soft Matter. *Adv. Funct. Mater.* **2010**, *20*, 2550−2564.

(35) Guvendiren, M.; Burdick, J. A.; Yang, S. Solvent Induced Transition from Wrinkles to Creases in Thin Film Gels with Depth-Wise Crosslinking Gradients. *Soft Matter* **2010**, *6*, 5795−5801.

(36) Zhang, Y.; Xue, J.; Li, D.; Li, H.; Huang, Z.; Huang, Y.; Gong, C.; Long, S.; Li, X. Tough Hydrogels with Tunable Soft and Wet Interfacial Adhesion. *Polym. Test.* **2021**, *93*, 106976.

(37) Gu, Z.; Wan, X.; Lou, Z.; Zhang, F.; Shi, L.; Li, S.; Dai, B.; Shen, G.; Wang, S. Skin Adhesives with Controlled Adhesion by Polymer Chain Mobility. *ACS Appl. Mater. Interfaces* **2019**, *11*, 1496−1502.

(38) Wang, S.; Fang, Y.; He, H.; Zhang, L.; Li, C. A.; Ouyang, J. Wearable Stretchable Dry and Self-Adhesive Strain Sensors with Conformal Contact to Skin for High-Quality Motion Monitoring. *Adv. Funct. Mater.* **2021**, *31*, 2007495.

(39) Zhao, Z. J.; Shin, S. H.; Lee, S. Y.; Son, B.; Liao, Y.; Hwang, S.; Jeon, S.; Kang, H.; Kim, M.; Jeong, J. H. Direct Chemisorption-Assisted

https://doi.org/10.1021/acsnano.2c05159
ACS Nano 2022, 16, 18157−18167

Nanotransfer Printing with Wafer-Scale Uniformity and Controllability. *ACS Nano* **2022**, *16*, 378−385.
(40) Park, W. I.; Park, T. W.; Choi, Y. J.; Lee, S.; Ryu, S.; Liang, X.; Jung, Y. S. Extreme-Pressure Imprint Lithography for Heat and Ultraviolet-Free Direct Patterning of Rigid Nanoscale Features. *ACS Nano* **2021**, *15*, 10464−10471.
(41) Zhao, Z.-J.; Hwang, S. H.; Kang, H.-J.; Jeon, S.; Bok, M.; Ahn, S.; Im, D.; Hahn, J.; Kim, H.; Jeong, J.-H. Adhesive-Layer-Free and Double-Faced Nanotransfer Lithography for a Flexible Large-Area Metasurface Hologram. *ACS Appl. Mater. Interfaces* **2020**, *12*, 1737−1745.
(42) Hwang, S. H.; Jeon, S.; Kim, M. J.; Choi, D.-G.; Choi, J. H.; Jung, J.-Y.; Kim, K.-S.; Lee, J.; Jeong, J. H.; Youn, J. R. Covalent Bonding-Assisted Nanotransfer Lithography for the Fabrication of Plasmonic Nano-Optical Elements. *Nanoscale* **2017**, *9*, 14335−14346.
(43) Bok, M.; Zhao, Z.-J.; Hwang, S. H.; Jeong, Y.; Ko, J.; Ahn, J.; Lee, J. H.; Jeon, S.; Jeong, J.-H. Biocompatible All-in-One Adhesive Needle-Free Cup Patch for Enhancing Transdermal Drug Delivery. *ACS Appl. Mater. Interfaces* **2021**, *13*, 58220−58228.
(44) Zhang, X.; Chen, G.; Yu, Y.; Sun, L.; Zhao, Y. Bioinspired Adhesive and Antibacterial Microneedles for Versatile Transdermal Drug Delivery. *Research* **2020**, *2020*, 3672120.

Recommended by ACS

Rapid Printing and Patterning of Tough, Self-Healable, and Recyclable Hydrogel Thin-Films toward Flexible Sensing Devices

Haili Qin, Shu-Hong Yu, *et al.*

OCTOBER 03, 2022
NANO LETTERS

READ

Molecular Rationale for the Design of Instantaneous, Strain-Tolerant Polymeric Adhesive in a Stretchable Underwater Human–Machine Interface

Yeonsun Choi, Mikyung Shin, *et al.*

JANUARY 10, 2022
ACS NANO

READ

A Solvent-Free Photochemical Route to Clickable Multifunctional Polyacrylic Elastomers

Hongyu Yan, Yuechuan Wang, *et al.*

JULY 18, 2022
ACS APPLIED POLYMER MATERIALS

READ

Poly(propylene fumarate)-Based Adhesives with a Transformable Adhesion Force for Suture-Free Fixation of Soft Tissue Wounds

Xin Guan, Dagang Guo, *et al.*

MARCH 02, 2022
ACS APPLIED POLYMER MATERIALS

READ

Get More Suggestions >

https://doi.org/10.1021/acsnano.2c05159
ACS Nano 2022, 16, 18157−18167